DOI: 10.1002/JLB.2VMA0118-008R

JLB JOURNAL OF LEUKOCYTE BIOLOGY

ARTICLE

CCL19 with CCL21-tail displays enhanced glycosaminoglycan binding with retained chemotactic potency in dendritic cells

Astrid S. Jørgensen[1] | Pontian E. Adogamhe[2] | Julia M. Laufer[3] | Daniel F. Legler[3] | Christopher T. Veldkamp[2] | Mette M. Rosenkilde[1] | Gertrud M. Hjortø[1]

[1]Department of Biomedical Sciences, Faculty of Health and Medical Sciences, The Panum Institute, University of Copenhagen, Copenhagen, Denmark

[2]Department of Chemistry, University of Wisconsin-Whitewater, Whitewater, Wisconsin, USA

[3]Biotechnology Institute Thurgau (BITg), at the University of Konstanz, Kreuzlingen, Switzerland

Correspondence
Gertrud M. Hjortø, Department of Biomedical Sciences, Faculty of Health and Medical Sciences, The Panum Institute, University of Copenhagen, Copenhagen DK-2200, Denmark.
Email: ghjortoe@sund.ku.dk

Abstract

CCL19 is more potent than CCL21 in inducing chemotaxis of human dendritic cells (DC). This difference is attributed to 1) a stronger interaction of the basic C-terminal tail of CCL21 with acidic glycosaminoglycans (GAGs) in the environment and 2) an autoinhibitory function of this C-terminal tail. Moreover, different receptor docking modes and tissue expression patterns of CCL19 and CCL21 contribute to fine-tuned control of CCR7 signaling. Here, we investigate the effect of the tail of CCL21 on chemokine binding to GAGs and on CCR7 activation. We show that transfer of CCL21-tail to CCL19 ($CCL19^{CCL21\text{-}tail}$) markedly increases binding of CCL19 to human dendritic cell surfaces, without impairing CCL19-induced intracellular calcium release or DC chemotaxis, although it causes reduced CCR7 internalization. The more potent chemotaxis induced by CCL19 and $CCL19^{CCL21\text{-}tail}$ compared to CCL21 is not transferred to CCL21 by replacing its N-terminus with that of CCL19 ($CCL21^{CCL19\text{-}N\text{-}term}$). Measurements of cAMP production in CHO cells uncover that CCL21-tail transfer ($CCL19^{CCL21\text{-}tail}$) negatively affects CCL19 potency, whereas removal of CCL21-tail ($CCL21^{tailless}$) increases signaling compared to full-length CCL21, indicating that the tail negatively affects signaling via cAMP. Similar to chemokine-driven calcium mobilization and chemotaxis, the potency of CCL21 in cAMP is not improved by transfer of the CCL19 N-terminus to CCL21 ($CCL21^{CCL19\text{-}N\text{-}term}$). Together these results indicate that ligands containing CCL21 core and C-terminal tail (CCL21 and $CCL21^{CCL19\text{-}N\text{-}term}$) are most restricted in their cAMP signaling; a phenotype attributed to a stronger GAG binding of CCL21 and defined structural differences between CCL19 and CCL21.

KEYWORDS

bias signaling, cAMP, chimera, migration, species bias, tail truncation

1 | INTRODUCTION

The chemokine receptor CCR7 plays an essential role guiding both innate and acquired immune responses. During immune cell activation, CCR7 controls CCL21 directed migration of both matured dendritic cells (DC, professional antigen-presenting cells) and naïve T cells to the lymph nodes (LN),[1] but also coordinates the subsequent encountering of antigen-presenting DCs with naïve T cells in the LN. Thus LN stromal cell secreted CCL19 and CCL21 are both important for orchestrating initial contacts between DCs and naïve T cells in LN T-cell zones as well as for stimulating chemokinesis of T-cells within LN.[2,3] On the other hand, autocrine CCL19 secretion by DCs may play a role in short-lived CCL19 guiding of the DC:T cell scanning process,[4–6] with the short-time span of CCL19 signaling compared to CCL21, making it ideal for this purpose. It is becoming increasingly clear that the two endogenous ligands that govern signaling via CCR7, CCL21 (also known as SLC)[7] and CCL19 (also known as ELC)[8] contribute to different aspects of immune cell function.[9] A different expression pattern of CCL19 and CCL21 may partly explain the different actions of these chemokines. Although both chemokines are secreted by LN stromal cells,[10] only CCL21 is presented by lymphatic endothelial cells and CCL19 is specifically being secreted by LN residing DCs.[11–13] Earlier as well as

Abbreviations: 3D, three-dimensional; BBXB, basic basic X basic; BRET, bioluminescence resonance energy transfer; CHO, Chinese hamster ovary; CI, chemotactic index; DC, dendritic cell; GAG, glycosaminoglycan; GRK, G protein-coupled receptor kinase; HEK, human embryonic kidney; HS, heparan sulfate; IP_3, inositol triphosphate; LN, lymph node; moDC, monocyte derived DC; NMR, nuclear magnetic resonance; RP, reverse phase; RT, room temperature

Received: 5 January 2018 | Revised: 13 March 2018 | Accepted: 13 March 2018

recent studies have provided evidence that these ligands are also functionally distinct signaling molecules. CCL19 seems to be more potent in inducing β-arrestin 2 recruitment and CCR7 internalization in various established cell lines, and, importantly, a more potent chemotactic cue in guiding DC chemotaxis compared to CCL21.[14–18] In contrast, CCL21 seems to be as strong as or stronger than CCL19 in inducing intracellular calcium release and ERK activation in DCs.[14,19,20] Thus CCL19 and CCL21 give rise to biased CCR7 signaling[9]; a phenomenon not only observed in CCR7, but also among other chemokine receptors.[21–23]

Chemokines are named according to the position of two conserved cysteines and are divided into 2 major groups, the CC and the CXC chemokines. CX_3CL1 separates itself from the rest by the conserved cysteines being separated by 3 amino acids. XCL1 and XCL2 differ by lacking one of the two conserved N-terminal cysteines and they therefore only form 1 cysteine bridge, in contrast to the rest of the chemokines that form 2 disulphide bridges with 2 conserved cysteines located in the core domains of the chemokines. CCL21 has 2 additional cysteines in its C-terminus (thus 6 in total) and forms a third cysteine bridge.[24]

Chemokine induced receptor activation relies on docking of the ligand N-terminus deep into the receptor binding pocket.[25,26] Since CCL19 and CCL21 have different N-termini, they are expected to interact with and thus activate CCR7 in different ways. Earlier studies have presented data on the interaction of CCL19 and CCL21 with CCR7.[14,27,28] Altogether these studies support different docking modes of the two chemokines, with specific amino acid residues in the receptor being differentially important for activation by one ligand and without affecting activation by the other. Thus amino acids in the top of transmembrane segment (TM)3 and TM4, in the area of the major binding pocket (encircled by TM3-7) are exclusively important for CCL21 induced CCR7 activation.[14] Recent modeling of CCL19 and CCL21 interactions with CCR7 suggests that CCL19 also makes ligand specific contacts with CCR7.[28]

Furthermore, CCL19 and CCL21 only display 32% sequence identity and differ in length with CCL21 encoding a 37 amino acid long C-terminal tail extension that is lacking in CCL19, giving rise to significant differences in GAG affinity.[29–31] We have previously shown that CCL21 is captured on the surface of human monocyte derived DCs (moDCs) to a much higher extent than CCL19, a characteristic that is dependent on the basic C-terminal tail of CCL21. This extensive GAG binding is hypothesized to disturb both gradient sensing in three-dimensional (3D) chemotaxis and the immediate availability of the ligand for receptor interaction and signaling.[14]

Finally, as described by Kiermaier et al., the tail of CCL21 seems to further control the chemokine activity, keeping it in an autoinhibited form, potentially through the tail folding back on the core domain, to be unlocked only upon binding to polysialic acid residues on CCR7, that is therefore of importance for CCL21 induced CCR7 activity in DCs where the polysialylation process is known to occur.[32]

Regulation of CCL21 activity through regulation of GAG affinity and relief of CCL21 intramolecular tail autoinhibition are highly relevant physiological events, as both DC-released proteases and plasmin have been shown to cleave the tail of CCL21 to generate $CCL21^{tailless}$ in vitro and in vivo.[33,34] The direct contribution of the CCL21-tail to ligand-specific cell surface binding and receptor activation profile has not been investigated before, but is an important aspect in understanding the differential activation modes of CCL19 and CCL21, which will allow future interference with ligand subsets.

We therefore set out to determine the effect of CCL21-tail cell surface binding, on chemokine induced 3D chemotaxis and CCR7-mediated signal transduction, employing various chimeric CCR7 binding chemokines together with endogenous CCL19, CCL21 and $CCL21^{tailless}$ to investigate the consequence of presence versus absence of a basic tail originating from CCL21. Chimeric ligand versions include CCL19 fused to the C-terminus of CCL21 ($CCL19^{CCL21\text{-}tail}$) and a CCL21 version where the first 16 amino acids have been substituted by CCL19 specific residues ($CCL21^{CCL19\text{-}N\text{-}term}$). The latter chimera was created to determine whether the N-terminus of CCL19 can potentiate the otherwise weaker CCL21-induced signaling through alteration of CCR7 docking.

2 | MATERIALS AND METHODS

2.1 | Materials

X-vivo 15 medium was from Lonza (Basel, Switzerland). $CaCl_2$, $MgCl_2$, Glucose, HEPES, human Ab serum, Na_2HCO_3 (7.5%), MEM (10X), FBS, penicillin/streptomycin, glutamine, PGE2, forskolin, formaldehyde, and fluoromount were from Sigma (St. Louis, MO, USA). IL-4, GM-CSF, TNF-α, IL-1β, and IL-6 were from Peprotech (Rocky Hill, NJ, USA). DMEM, RPMI, PBS, Trypsin, and HBSS were from Thermo Scientific (Gibco)(Watham, MA, USA). Lymphoprep was from STEMCELL technologies (Vancouver, Canada). PureCol Bovine Collagen I suspension was from Advanced Biomatrix (Carlsbad, CA, USA). CCL19 (catalog No. 361-MI), CCL21 (catalog No. 366-6C), and anti-CCL19 (catalog No. AF-361) were from R&D Systems (Minneopolis, MN, USA). $CCL21^{tailless}$ (CCL21 amino acids 1–79) was from Almac (Craigavon, Nothern Ireland). Donkey anti goat Alexa488 Ab was from Thermo Scientific (Molecular probes; Watham, MA, USA). Rabbit anti goat HRP coupled Ab was from Bio-Rad (Hercules, CA, US). Maxisorp plates from NUNC (WVR catalog No. 442404). Anti-CCR7 Ab was from eBiosciences (San Diego, CA, USA). Coelenterazine was from Nanoligth technologies (Pinetop, AZ, USA). Ibidi 3D chemotaxis slides were from Ibidi (Martinsried, Germany). Probenicid and Fluo-4 were from Thermo Scientific (Invitrogen; Watham, MA, USA). Standard chemicals used for protein expression were from Sigma (St. Louis, MO, USA). His60 nickel resin was from Clontech (Mountain View, California, USA). SP HP HiTrap™ column was from GE Healthcare (Chicago, IL, USA).

2.2 | Expression and purification of the human chimeric $CCL19^{CCL21\text{-}tail}$ and $CCL21^{CCL19\text{-}N\text{-}term}$ chemokines

Synthetic DNA coding for either an SMT3-full length CCL19, residues1-77, and CCL21 residues 78–111 fusion protein (SMT3-$CCL19^{CCL21\text{-}tail}$) or an SMT3-CCL19 residues 1–16 and CCL21 residues 17–111 fusion protein (SMT3-$CCL21^{CCL19\text{-}N\text{-}term}$) was cloned

into the BamHI and Hind III sites of pET28a. Expression plasmids were transformed into BL21 [DE3] *Escherichia coli*. The constructs are designed to produce proteins with the following amino acid sequences.

CCL19 residues 1–77 CCL21 residues 78–111 ($CCL19^{CCL21\text{-}tail}$): GTNDAEDCCL SVTQKPIPGY IVRNFHYLLI KDGCRVPAVV FTTLRGRQLC APPDQPWVER IIQRLQRTSA KMKRRSSQGC RKDRGASKTG KKGKGSKGCK RTERSQTPKG P

CCL19 residues 1–16 CCL21 residues 17–111 ($CCL21^{CCL19\text{-}N\text{-}term}$): GTNDAEDCCL SVTQKPIPAK VVRSYRKQEP SLGCSIPAIL FLPRKRSQAE LCADPKELWV QQLMQHLDKT PSPQKPAQGC RKDRGASKTG KKGKGSKGCK RTERSQTPKG P

One-liter cultures were grown at 37°C in lysogeny broth, or in the case of $CCL19^{CCL21\text{-}tail}$ either lysogeny broth or [U-^{15}N/^{13}C] M9 minimal media to an optical density of 0.5–0.7 at 600 nm. Recombinant protein expression was then induced with 1 mM isopropyl-β-D-thiogalactopyranoside for 5 h. Cell pellets were collected by centrifugation and stored at −20°C. Cells were resuspended in 10 mL of buffer A (50 mM sodium phosphate, 300 mM NaCl, 10 mM imidazole, pH 8.0) containing 1 mM PMSF and 0.1% (v/v) 2-mercaptoethanol. Resupended cells were lysed by sonication which was followed by centrifugation at 15,000 × *g* for 15 min. The pelleted inclusion body containing the His_6-SMT3-chimera was dissolved in 10 mL of buffer AD (50 mM sodium phosphate, 300 mM NaCl, 10 mM imidazole, and 6 M guanidine hydrochloride, 0.1% (v/v) 2-mercaptoethanol, pH 8.0), clarified by centrifugation at 15,000 × *g* for 15 min and batch loaded onto 2 mL of His60 nickel resin for 30 min. The column was washed with 40 mL of buffer AD and eluted with 30 mL of buffer BD (100 mM sodium acetate, 300 mM NaCl, 10 mM imidazole, and 6 M guanidine hydrochloride, pH 4.5). Elutions were pooled and dialyzed against 4 L of 20 mM TRIS pH 8.0 overnight and then transferred to a fresh 4 L of 20 mM TRIS pH 8.0. A total of 400 μg ubiquitin like protease-1 was added to the dialysate and left to digest the His_6-SMT3-chimera at 4°C until complete digestion was observed by SDS-PAGE. After clarification by centrifugation at 4000 × *g* for 15 min, the digestion was loaded onto an SP HP HiTrap™ 1 mL column at 1 mL per minute. The column was then washed with 15 mL of wash buffer (100 mM TRIS, 25 mM NaCl, pH 8.0), and eluted with 15 mL of elution buffer (100 mM TRIS, 2 M NaCl, pH 8.0). The chimera was further purified using reverse phase (RP) HPLC (C18 column, 0.1% aqueous trifluoroacetic acid buffer with a CH_3CN gradient from 21 to 42% (v/v) over 30 min). Purity, identity, and folding were verified by a combination of SDS-PAGE, RP-HPLC, mass spectrometry, and protein nuclear magnetic resonance (NMR) similar to Veldkamp *et al.*[35] For example, in Supplemental Fig. S1 ^{1}H spectra of $CCL21^{CCL19\text{-}N\text{-}term}$ show chemical shift dispersion indicating a folded chemokine and reduction results in a spectrum showing degenerate chemical shifts consistent with an unfolded protein.[35] Additionally, ^{15}N-^{1}H heteronuclear single quantum coherence spectra (HSQC) of uniformly ^{15}N/^{13}C labeled $CCL19^{CCL21\text{-}tail}$, as seen in Supplementary Fig. S2, indicate this chimera is folded and that there are significant similarities between the corresponding CCL19 and CCL21 regions of this chimera and HSQC spectra of either CCL19[36] or residues corresponding to the tail of CCL21.[24] Protein NMR data was collected at the Medical College of Wisconsin's NMR facility as previously described.[35]

2.3 | DCs preparation

DCs were prepared from human PBMCs isolated from buffy coats by centrifugation on a Lymphoprep gradient. Briefly monocytes were isolated by plastic adherence of PBMC. Adhered monocytes were subsequently cultured and differentiated into immature DCs by incubation with IL-4 (250 U/mL) and GM-CSF (1000 U/mL) for 6 d, followed by activation into mature DCs by incubation with IL-6 (1000 U/mL), IL-1β (1000 U/mL),TNF-α (1000 U/mL), and PGE2 (1 μg/mL) for an additional 2 d in the same medium.

2.4 | Cell culturing

Human DCs were grown in X-vivo 15 medium with 2% human AB serum and Glutamine. CHO-K1 cells were grown in RPMI with 10%FBS and penicillin/streptomycin. All cells were split routinely by dislodging in trypsin. All cells were kept in a humidified incubator at 37°C, 5% CO_2. For stable cell-lines the passage number did not exceed 40.

2.5 | 3D chemotaxis

Chemotaxis assays were conducted as previously described.[14] Briefly, mature human moDCs were thawed and allowed to acclimatize by resting in medium for 30 min at room temperature (RT) before assay start. DCs were seeded in bovine collagen I mixture prepared by mixing Na_2HCO_3 (7.5%), MEM (10×), collagen 1 solution (1:2:15), and DCs dissolved in X-vivo 15 medium (2×10^6 cells/mL) in the ratio 1:2:15:9. After polymerization for 45 min in a humidified incubator at 37°C (5% CO_2), the source and sink reservoirs were filled according to the manufacturer's instructions and the migration was tracked in a time-lapse microscope with a humidified temperature controlled stage incubator for 12 h at a 2 min interval. Cell migration (approximately 20–40 cells per viewing field) was tracked using a commercial tracking program (Autozell) and subsequently analyzed to get a population-based chemotactic index (CI) value (MATLAB). CI is a measure of net translocation distance to the source relative to total distance traveled and was thus calculated as the ratio of the distance traveled in the direction of the gradient over the total distance traveled and therefore is a conservative measure of the directedness of cell migration. Without any chemokine (no induction of directed migration) the basal migration should have a CI close to zero, meaning that the cells move randomly in all directions to the same degree (meaning no overall movement in any direction). Theoretically, the maximal CI would be 1, meaning that every displacement of the cell is in the direction of the source (this is not observed in praxis).

2.6 | Ligand DC surface staining

Thawed DCs were left to acclimatize in X-vivo 15 medium with 2% human Ab serum and glutamine for half an hour. DCs were divided in 3 vials, 200 μL each at a concentration of 1×10^6 cells/mL. DCs were stored on ice for 20 min. Chemokine buffer (negative control), CCL19 (100 nM), or $CCL19^{CCL21\text{-}tail}$ chimera (100 nM) was added on ice for 30 min. DCs were washed once in ice-cold PBS 0.5% BSA and twice in ice-cold PBS, and fixed in 3.7% formaldehyde in PBS for 10 min on ice

and then 10 min at RT. DCs were washed 3 times in PBS 1% BSA and incubated in PBS 1% BSA for 20 min at RT. Primary goat anti human CCL19 Ab was added (final concentration 4 μg/mL in PBS 1% BSA) and the DCs were left to stain at RT for 45 min. The primary Ab was removed and the DCs were washed 3 times in PBS, and stained with secondary Ab donkey anti goat Alexa-488 in PBS 1% BSA, for 45 min at RT in the dark.

The DCs were washed twice in PBS and once in milliQ water. The DCs were removed and dissolved in 70% ethanol, 25 μL per sample, and left to dry on microscope slide. Fluoromount was added and samples sealed under cover-glass nail polish.

2.7 | ELISA quantifying anti-CCL19 Ab reactivity toward CCL19 and CCL19$^{CCL21\text{-}tail}$

Maxisorp plates were coated with 100 μL CCL19 or CCL19$^{CCL21\text{-}tail}$ chimera diluted in PBS (final concentration 100 nM) at 4°C overnight with adhesive cover plastic.

On day 2, chemokine solution was removed and the plates were washed 3 times in PBS. Unspecific binding was blocked by incubation in PBS with 1.5% BSA for 1 h on shaking table at RT.

Plates were washed 3 times in PBS. Anti-CCL19 Ab was added to a final concentration of 2 μg/mL in PBS and the plates incubated at RT for 60 min. The primary Ab was removed and the plates were washed 3 times in PBS. Secondary HRP coupled rabbit-anti goat Ab was added in PBS and the plates were incubated at RT for 90 min. The plates were finally washed 3 times in PBS and 3,3′,5,5′-tetramethylbenzidine (TMB) detection added for 5–10 min. The reaction was stopped by adding 2 mM H_2SO_4 and the plates were read in an ELISA plate reader.

2.8 | Flow-cytometry determination of ligand induced CCR7 internalization

DCs were stimulated for 30 min with medium or 1, 10, or 100 nM of CCL19, CCL21, or CCL19$^{CCL21\text{-}tail}$ chimera at 37°C and remaining CCR7 surface expression was determined (mean fluorescence intensity) by flow cytometry as described previously.[37] From all experiments the percentage of remaining CCR7 surface expression was calculated after chemokine-mediated receptor internalization in relation to CCR7 surface expression of cells incubated with medium alone. As control, cells were incubated for 30 min with 100 nM CCL19, CCL21, or CCL19$^{CCL21\text{-}tail}$ at 4°C to show that chemokine binding to CCR7 does not affect binding of the CCR7 specific Ab used to determine receptor internalization.

2.9 | Calcium signaling

DCs were seeded in a poly-D-lysine coated white 96-well iso plate (80,000 cells per well) and allowed to adhere for 2 h. Medium was removed and the DCs incubated in HEPES (20 mM) buffered HBSS with 1 mM $CaCl_2$, 1 mM $MgCl_2$, 250 μL probenicid, and 0.4% Fluo-4 in the dark at 37°C for 60 min.

Fluo-4 buffer was removed and the cells were washed twice in the same buffer without Fluo-4. The DCs were left in this buffer and transferred to heated (37°C) Flex-station reader for automated pipetting of ligands and detection of real-time changes in Fluo-4 fluorescence reflecting changes in intracellular calcium.

2.10 | Bioluminescence resonance energy transfer (BRET) cAMP assay

CHO cells were seeded in a 6-well plate, 500,000 cells/well, and transiently co-transfected with vectors encoding the WT human CCR7 and Camyel sensor[38] in a 1:5 ratio using Lipofectamine 2000 (6 μg/well). The following day cells were resuspended in PBS with glucose and seeded in 96-well black/white iso plate (~25,000 cells/well). Coelenterazine (camyel bioluminescence substrate) was added to a final concentration of 5 μM. After 10 min, cells were stimulated with varying ligand concentrations for a total of 40 min. Forskolin was added to each well 5 min after ligand addition to reach a final concentration of 5 μM. The plates were kept in the dark at all times. Emission signal from Rluc and YFP was measured using the envision machine at 530 and 480 nm and the BRET signal determined as the ratio between enhanced Yellow Fluorescent Protein/ Renilla Luciferase (eYFP/Rluc). BRET camyel sensor concept: The camyel molecule is made up of: Rluc, YFP, and the cAMP-binding molecule EPAC. At Low cAMP, camyel is in a conformation, where the Rluc excites YFP, leading to high emission of 525 nm and high eYFP/Rluc ratio. At high cAMP, camyel is in a conformation, where the Rluc and YFP are far from each other, meaning no cross-excitation and thus low 525 nm emission and low ratio.

2.11 | Statistical analysis

Error bars are indicated as SEM. Statistical analysis performed are *t*-test and *P*-values < 0.01 indicated by ** and P values < 0.05 indicated by *. Non-significant differences are indicated by NS.

3 | RESULTS

3.1 | CCL21-tail transfer to CCL19 (CCL19$^{CCL21\text{-}tail}$) increases surface binding to dendritic cells

It has previously been shown that removal of the extended basic C-terminal tail of CCL21 prevents the otherwise strong binding of CCL21 to the DC cell surface.[14] The CCL21-tail harbors 2 basic BBXB domains that convey affinity for acidic GAGs in the extracellular environment and on the cell membrane. To access the role of the tail in cell-surface binding, we used a chimeric version of CCL19, CCL19$^{CCL21\text{-}tail}$, containing the C-terminal tail (amino acids 78–111) of CCL21 (Fig. 1A). Human moDCs were incubated on ice with either CCL19 or CCL19$^{CCL21\text{-}tail}$ and the amount of ligand binding to cell surfaces over a fixed time period was subsequently determined via detection with fluorescently labeled antibodies. In contrast to CCL19 (Fig. 1A), CCL19$^{CCL21\text{-}tail}$ binds profoundly to the surface of human mature moDCs (Fig. 1B). We used a commercially available Ab raised against CCL19 to detect both ligands. The Ab recognized both wild type CCL19 and CCL19$^{CCL21\text{-}tail}$ as evaluated by ELISA (Fig. 1C).

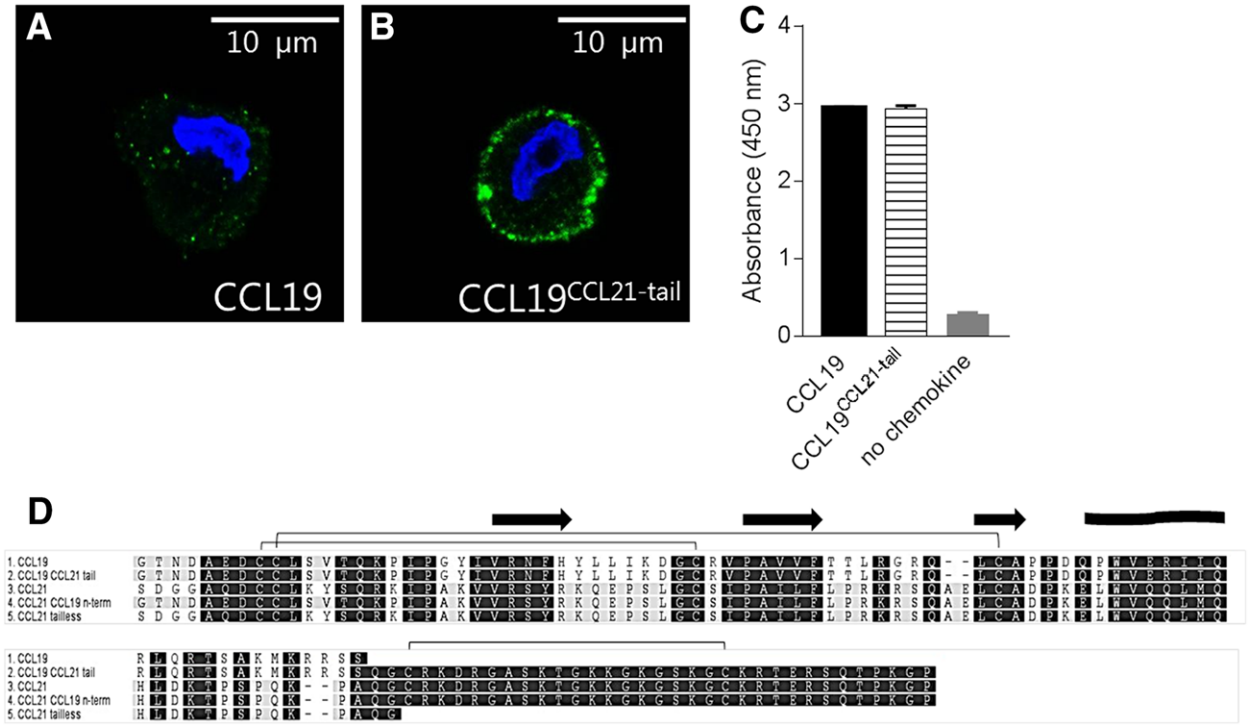

FIGURE 1 **Introducing the basic C-terminal tail of CCL21 onto CCL19 affects its GAG binding ability and surface interaction with DCs**. Introducing the tail of CCL21 onto CCL19 causes its distinct binding to the surface of human mature moDCs (B) to a much higher extent than wild type CCL19 (A). The Ab used detects CCL19$^{CCL21\text{-}tail}$ to the same degree as it detects CCL19 as estimated via ELISA on adsorbed ligands (C). Overview of wild type and chimeric CCR7 ligands used in this study (D), with cysteines bridges indicated with lines between the connected cysteines, and secondary structures above with beta-sheets shown as arrows and the alpha-helix as a banner. CCL21^{tailless} lacks 2 cysteines in the C-terminus compared to CCL21 and thus only forms 2 cysteine bridges. (Ligand surface staining's (Fig. 1A and B) and ELISA data (Fig. 1 C) represent data from three separate experiments ($n = 3$))

Since antigen detection in ELISA is different from antigen detection in immune histochemistry (IHC), this is a rough estimate of how well the Ab detects CCL19$^{CCL21\text{-}tail}$ compared to CCL19. The different wild type and chimeric chemokine versions tested throughout this study are depicted in a schematic illustration in Fig. 1D.

3.2 | CCL21-tail transfer to CCL19 (CCL19$^{CCL21\text{-}tail}$) does not lower the chemotactic potency of CCL19 in DCs

As described before, CCL21 is a less potent chemotactic signal compared to CCL19 for human and murine DCs.[14,20] To investigate whether the actual capture of CCL21-tail containing ligands on cell surface GAGs can be linked to a low chemotaxis inducing potency in DCs, we investigated whether the CCL21-tail transferred to CCL19 affected its chemotactic potential. Whereas CCL21 is less potent than CCL19, CCL19$^{CCL21\text{-}tail}$ is as potent as CCL19 in inducing chemotaxis in 3D, both in collagen I gels (Fig. 2A) and in more complex Matrigels (Fig. 2B). This indicates that chemokine cell surface binding is not a determining factor for chemotactic potency in vitro. Spiderweb diagrams of DC chemotaxis toward 10 nM of CCL21 (Fig. 2C), CCL19$^{CCL21\text{-}tail}$ (Fig. 2D), and CCL19 (Fig. 2E) (source to the left side) clearly demonstrate directed migration induced by CCL19$^{CCL21\text{-}tail}$ and CCL19, but not CCL21. Supplementary Movies illustrating this are supplied (Supplementary Movie 1–3).

3.3 | CCL21-tail transfer to CCL19 (CCL19$^{CCL21\text{-}tail}$) affects potency and efficacy of CCR7 internalization in DCs

CCL19 and CCL21 binding to CCR7 leads to recruitment of different GRKs that differentially affect β-arrestin recruitment and subsequent CCR7 internalization, with CCL21 inducing considerable less CCR7 internalization compared to CCL19.[14,15,17] Here, we investigate if the increased surface binding of CCL19$^{CCL21\text{-}tail}$ compared to CCL19 results in a change in CCR7 internalization pattern. For all chemokines we observed endocytosis in a concentration-dependent manner and experiments at 4°C using 100 nM of chemokine showed that chemokine binding to the receptor does not prevent Ab binding (Fig. 3). As expected, CCR7 was readily endocytosed after CCL19 stimulation. Stimulation with as little as 1 nM CCL19 already let to the internalization of about 30% of CCR7 whereas at 10 and 100 nM CCL19 about 50% of CCR7 was internalized (Fig. 3A). Compared to CCL19, CCL19$^{CCL21\text{-}tail}$ is less potent, especially at low concentrations, in inducing CCR7 endocytosis. Thus upon stimulation with 1 nM of CCL19$^{CCL21\text{-}tail}$ only 20% of CCR7 was internalized and a maximum of 40% CCR7 endocytosis was reached for 100 nM CCL19$^{CCL21\text{-}tail}$ (Fig. 3). For CCL21, at 1 nM only 10% of CCR7 was internalized and at 100 nM only 25% of CCR7 was endocytosed. Hence, CCL19$^{CCL21\text{-}tail}$ is more potent than CCL21, but not as potent as CCL19 in inducing CCR7 endocytosis (Fig. 3A) indicating that chemokine binding to

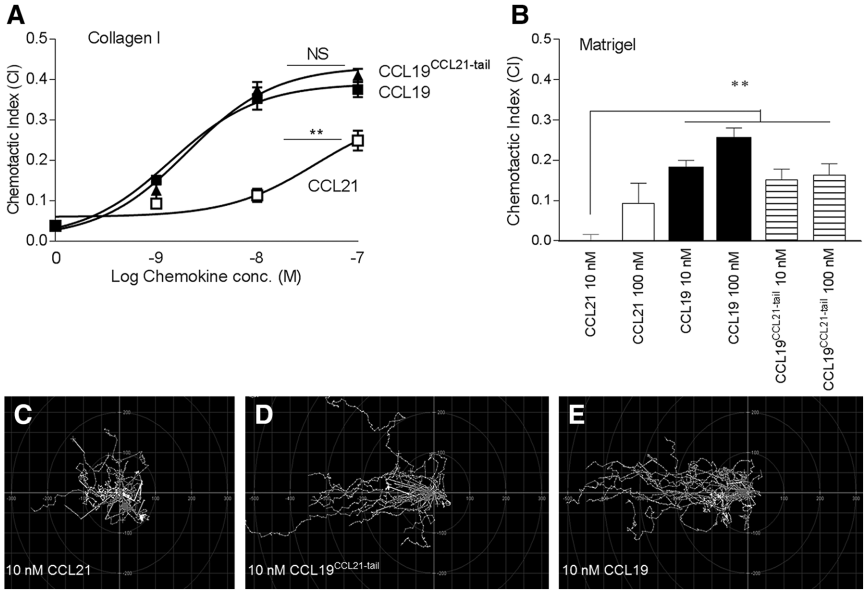

FIGURE 2 CCL19$^{CCL21\text{-}tail}$ and CCL19 are potent chemotactic signals. CCL19$^{CCL21\text{-}tail}$ resembles CCL19 with regard to chemotactic potency in human mature DCs in Collagen I (A) (CCL21 open squares, CCL19 closed black squares and CCL19$^{CCL21\text{-}tail}$ closed black triangles) (n = 3–11) and in Matrigel (n = 3–5)(B). Spiderweb diagrams of DC chemotaxis toward 10 nM CCL21 (C), 10 nM CCL19$^{CCL21\text{-}tail}$ (D) and 10 nM CCL19 (E)

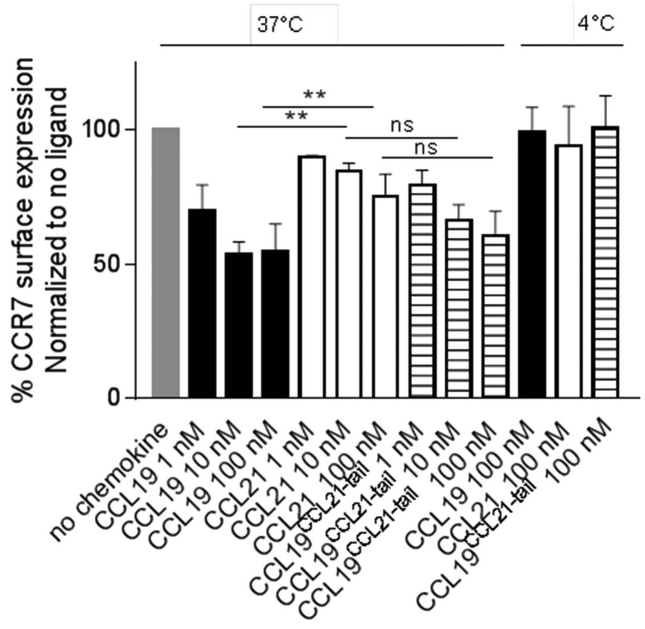

FIGURE 3 Introducing the basic C-terminal tail of CCL21 onto CCL19 does not affect its ability to direct CCR7 internalization. moDCs were stimulated for 30 min with indicated concentrations of CCL19, CCL21, and CCL19$^{CCL21\text{-}tail}$ at 37°C or with 100 nM of the indicated chemokines at 4°C. Error bars represent Mean ± SEM (n = 3–7)

cell surface GAGs at least partially interferes with ligand induced receptor internalization.

3.4 | CCL21-tail transfer to CCL19 (CCL19$^{CCL21\text{-}tail}$) does not affect CCL19-induced signaling via changes in intracellular calcium release in DCs

The fact that CCL19$^{CCL21\text{-}tail}$ behaves like CCL21 with regard to DC surface binding, but like CCL19 with regard to chemotaxis and intermediate in receptor internalization spurred us to investigate if signaling via downstream pathways was influenced by the transfer of CCL21-tail to CCL19. Thus, we measured intracellular calcium release in response to CCL21, CCL19, and CCL19$^{CCL21\text{-}tail}$ in human moDCs and found that CCL19$^{CCL21\text{-}tail}$ resembles neither CCL19 nor CCL21 with regard to inducing intracellular calcium mobilization (Fig. 4A–D). Overall, CCL21 induces intracellular calcium release with both higher potency and higher efficacy compared to CCL19, with CCL19$^{CCL21\text{-}tail}$ reaching a level somewhere in between (Fig. 4D). These data show that the higher potency of CCL19 and CCL19$^{CCL21\text{-}tail}$ in terms of controlling chemotaxis does not correlate with the potency of these chemokines in mobilization of intracellular calcium.

3.5 | CCL19 N-terminus transfer to CCL21 (CCL21$^{CCL19\text{-}N\text{-}term}$) does not rescue the low chemotactic potency of CCL21 in DCs

We wondered if the higher potency of CCL19 and CCL19$^{CCL21\text{-}tail}$ in chemotaxis, compared to CCL21, was conveyed by the N-terminus of CCL19 given the presumed different receptor docking mode of the N-termini of these ligands,[14] or whether the differences in activation profiles reside in the overall difference in the chemokine core structures. To test this, we employed another chimeric chemokine in which the first 16 N-terminal amino acids of CCL21 were exchanged with the equivalent part of CCL19, named CCL21$^{CCL19\text{-}N\text{-}term}$ (Fig. 5A). This chimera retained the poor potency of CCL21 in inducing chemotaxis of human DCs (Fig. 5B).

3.6 | CCL19 N-terminus negatively affects potency of CCL21 signaling via intracellular calcium release

Since CCL21$^{CCL19\text{-}N\text{-}term}$ resembled CCL21 with regard to chemotaxis inducing potential, we next tested the ability of this chimera to signal via changes in intracellular calcium. As previously shown (Fig. 4) CCL21, CCL19$^{CCL21\text{-}tail}$, and CCL19 are all potent in inducing intracellular calcium release, although CCL21 and CCL19$^{CCL21\text{-}tail}$ seem to be more efficient than CCL19 (Fig. 6C and D). CCL21$^{CCL19\text{-}N\text{-}term}$ on the other hand displays a significantly reduced activity through this

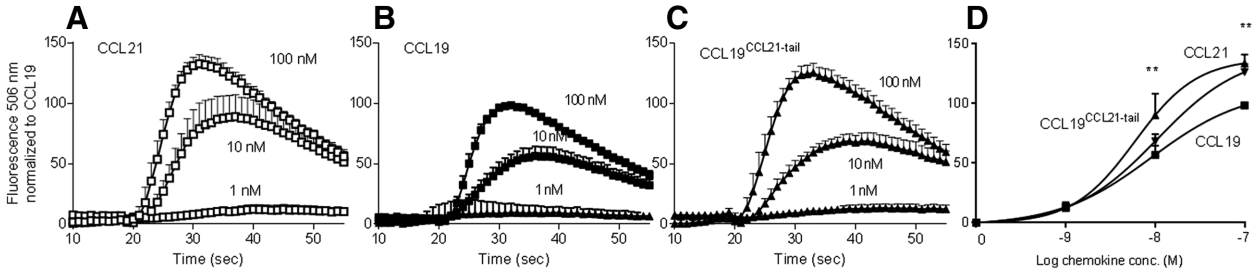

FIGURE 4 **Introducing the basic C-terminal tail of CCL21 onto CCL19 does not affect its ability to signal via calcium in human DCs**. Both CCL19 and CCL21 signal efficiently via calcium in human DCs. CCL19$^{CCL21\text{-}tail}$ retains this activity. Thus CCL21 tail does not significantly affect intracellular calcium release, all ligands are biologically active. The three ligands elicit similar responses at 1 nM, 10 nM, and 100 nM concentrations (A–C). CCL21 open squares, CCL19 closed black squares and CCL19$^{CCL21\text{-}tail}$ closed black triangles ($n = 6$–10). Dose response curves based on the maximal response elicited by the different chemokine concentrations (D), reveal that CCL21 is both more potent and more efficient than CCL19 in eliciting intracellular calcium release.

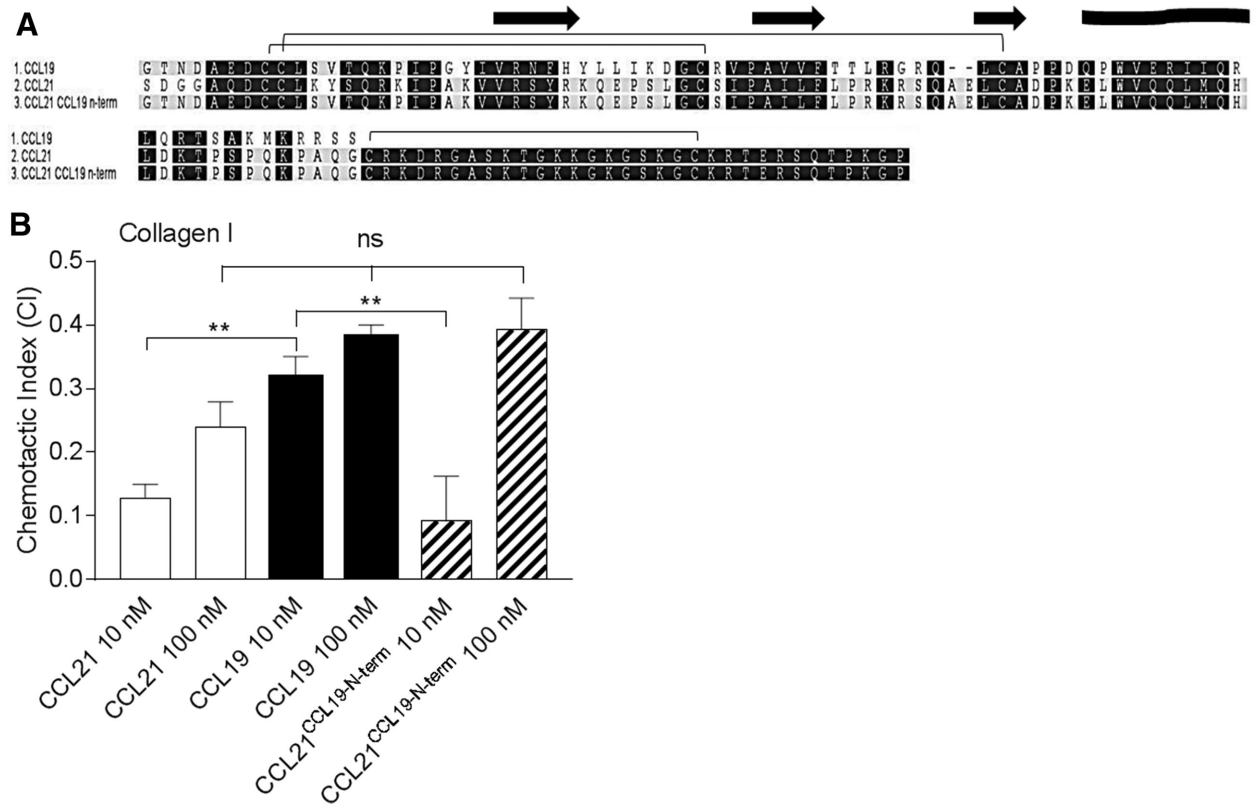

FIGURE 5 **The higher potency of CCL19$^{CCL21\text{-}tail}$ compared to CCL21 cannot be transferred to CCL21 by CCL19 N-terminus**. Overview of wild type and chimeric CCR7 ligands used in this assay (A). The CCL21$^{CCL19\text{-}N\text{-}term}$ chimera, in which the first 16 amino acids of CCL21 have been replaced with the first 16 amino acids of CCL19, retains the low potency of CCL21 in chemotaxis (B)($n = 4$)

pathway compared to both CCL21 and CCL19$^{CCL21\text{-}tail}$ (Fig. 6A, C, and D). Interestingly, CCL21^{tailless} is even less potent than CCL21$^{CCL19\text{-}N\text{-}term}$ (Fig. 6A, B, C, and D).

3.7 | CCL21-tail negatively affects signaling via changes in cAMP and CCL19 N-terminus is not able to rescue the poor potency of CCL21 derived ligands

Since the abilities of the tested chemokines to signal via calcium mobilization do not correlate with their chemotaxis inducing potential, we investigated whether $G_{\alpha i}$-signaling resulting in reduced cAMP production could be related to ligand potency controlling chemotaxis. We therefore tested the effect of CCL19, CCL19$^{CCL21\text{-}tail}$, CCL21, CCL21$^{CCL19\text{-}N\text{-}term}$, and CCL21^{tailless} for their ability to signal via cAMP. We used a BRET-based assay to measure decrease in cAMP, following $G_{\alpha i}$-mediated inhibition of forskolin-induced adenylate cyclase activity in transfectable CHO cells.

Our results show that transfer of CCL21-tail to CCL19 impairs its ability to signal via cAMP as CCL19$^{CCL21\text{-}tail}$ displays a 15-fold decreased potency compared to CCL19 (EC_{50} of 18.4 nM, log EC_{50} ± SEM: −7.74 ± 0.2 vs. EC_{50} of 1.14 nM, log EC_{50} ± SEM: −8.94 ± 0.12) (Fig. 7). On the other hand CCL19$^{CCL21\text{-}tail}$ is still

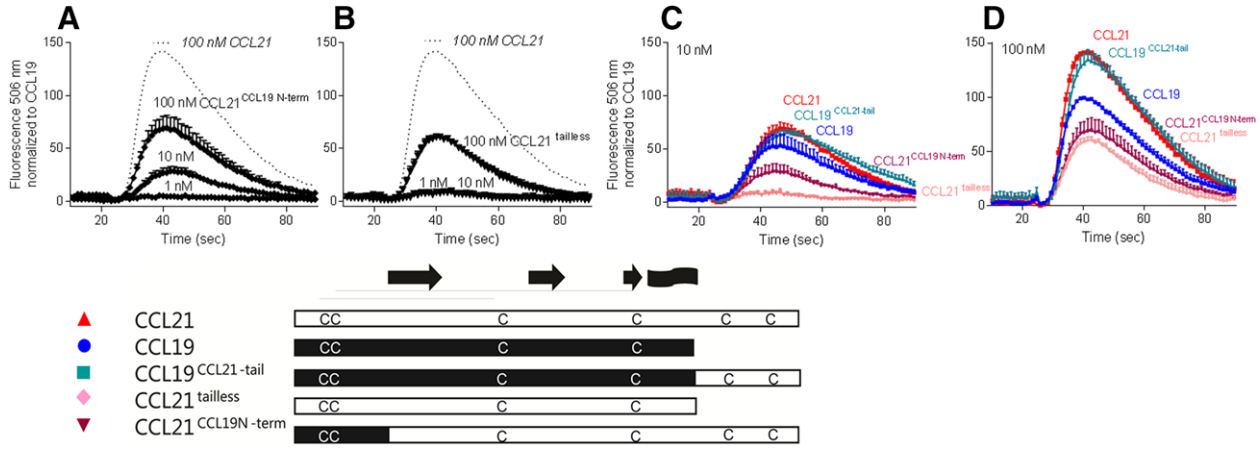

FIGURE 6 **CCL19 N-terminus negatively affects CCL21 induced signaling via calcium in human DCs, and tail removal reduces CCL21 potency even more.** As previously shown CCL21, CCL19$^{CCL21\text{-}tail}$, and CCL19 are all potent in inducing intracellular calcium release (Fig. 6A–C) with CCL21 and CCL19$^{CCL21\text{-}tail}$ displaying a significantly higher efficacy than CCL19 ($P \leq 0.01^{**}$ at 100 nM). On the other hand CCL21$^{CCL19\text{-}N\text{-}term}$ displays a significantly reduced activity through this pathway compared to both CCL21 and ($P \leq 0.01^{**}$ at 10 and 100 nM) and CCL19$^{CCL21\text{-}tail}$ ($P \leq 0.05^{*}$ and $P \leq 0.01^{**}$ at 10 and 100 nM, respectively). Interestingly, CCL21^{tailless} was even less potent than CCL21$^{CCL19\text{-}N\text{-}term}$ ($n = 3$–5)

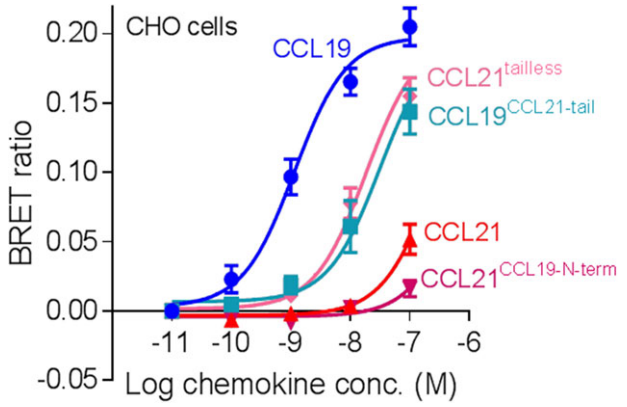

FIGURE 7 **The inhibitory effect on signaling via cAMP is driven by the CCL21 tail and further enhanced by the CCL21 core domain.** As with adding CCL21 tail to CCL19 (CCL19$^{CCL21\text{-}tail}$) resulting in decreased signaling, removing the tail of CCL21 results in improved signaling properties (CCL21^{tailless}) (Decrease in intracellular cAMP is reflected by an increase in BRET ratio) in CHO cells. CCL21$^{CCL19\text{-}N\text{-}term}$ displays low potency in cAMP signaling like CCL21 ($n = 3$)

more potent than CCL21 that displays a much lower potency (~15-fold) in cAMP signaling (estimated EC_{50} ~260 nM, log EC_{50} ± SEM: −6.57 ± 0.06) (Fig. 7).

We next addressed whether removal of the tail from CCL21 would increase its potency. Indeed, CCL21^{tailless} was improved approximately 15-fold in its ability to signal via cAMP compared to CCL21 and CCL21$^{CCL19\text{-}N\text{-}term}$ with a potency similar to CCL19$^{CCL21\text{-}tail}$ (EC_{50} of 12.5 nM, log EC_{50} ± SEM: −7.9 ± 0.12) (Fig. 7). This indicates that CCL21-tail alone negatively affects ligand induced signaling in this pathway.

Since both CCL21 and CCL21$^{CCL19\text{-}N\text{-}term}$ display low potency in this assay, it seems that the tail together with CCL21 core domain has a negative influence on signaling via cAMP and that the ability to signal via this pathway may correlate with the chemotaxis inducing potency, where these ligands both display a similarly poor activity.

4 | DISCUSSION

Signaling bias is well established in the chemokine system.[39] For CCR7, there are some discrepancies across studies with regard to relative potencies of CCL19 and CCL21 in signaling via $G_{\alpha i}$ (probably reflecting the use of different cells and assay systems),[14] but CCL19 has consistently been proven to be more potent in inducing CCR7 phosphorylation, β-arrestin recruitment and internalization, in various established cell-lines and primary cells,[7,14,16–18] and has also been shown to be a more potent chemotactic signal for both murine and human DCs compared to CCL21.[14,20]

Based on our previous observations that CCL21 binds extensively to DC surfaces and is a poor chemotactic signal compared to CCL19, and that removal of the tail (CCL21^{tailless}) diminish surface gluing and rescue chemotaxis,[14] we hypothesized that the low potency of CCL21 could be attributable to its extensive surface binding, disturbing external gradient sensing and immediate ligand availability. In the present work, we investigate the effect of ligand cell surface binding via CCL21-tail on 3D chemotaxis and signaling properties, by employing various chimeric CCR7 ligands to investigate the consequence of presence versus absence of the tail. Most experiments were carried out in human moDCs, except studies on signaling via cAMP which were performed in CHO cells, due to the need for transfection when using the camyel sensor system.[38]

Strong GAG binding by CCL21 is a well-known phenomenon,[29,30,40] but the fact that it binds extensively to not only endothelial cells, but also to the surface of immune cells could potentially affect availability for receptor interaction, with different GAGs having different effects on receptor interaction and signaling. Interestingly, binding of CCL21 to chondroitin sulfate B has previously been shown to inhibit signaling via CCR7 whereas binding to heparan sulfate (HS) had no such inhibitory effect.[30]

Here we show that transfer of the CCL21-tail to CCL19 (CCL19$^{CCL21\text{-}tail}$) does not negatively affect CCL19's ability to induce chemotaxis in human DCs, despite the increased surface

binding of this chimera to DC surfaces, ruling out that binding to the cell surface per se interferes with chemotaxis. Our finding is consistent with a study by Barmore et al.[31] that reveals increased heparin binding by the same chimera, CCL19$^{CCL21\text{-}tail}$ compared to CCL19, which demonstrates that the basic C-terminal tail of CCL21 is enough to confer high GAG affinity. Interestingly, we show here, that CCR7 internalization driven by CCL19$^{CCL21\text{-}tail}$ decreased compared to CCL19 but is not as low as for CCL21, indicating that high GAG affinity somehow has an effect on the ability of CCR7 to internalize.

Furthermore, transfer of CCL21-tail to CCL19 (CCL19$^{CCL21\text{-}tail}$) potentiates intracellular calcium release in DCs, in which CCL19$^{CCL21\text{-}tail}$ and CCL21 tend to display higher efficacy compared to CCL19. This confirms that GAG binding by CCL21 (and CCL19$^{CCL21\text{-}tail}$) does not necessarily restrict signaling. CCL21^{tailless} exhibits a very low potency in calcium signaling in DCs, whereas it has previously been shown to be as potent as CCL19 in inducing chemotaxis of these cells[14] indicating that calcium signaling is not directly linked to chemotaxis.

Modeling of CCR7 ligand interactions by Gaieb et al.[41] indicates that CCL19 and CCL21 contacts CCR7 in different manners, with distinct electrostatic profiles of the ligands' N-termini affecting the interaction with the corresponding electrostatic regions in the receptors binding pocket. CCR7 harbors 2 distinct electrostatic binding pocket regions; the structure of CCL21 seems to enable interaction in both regions, whereas the presence of a negative charge (D4) in CCL19´s N-terminal domain seems to restrict its interaction compared to CCL21.

To test if the higher chemotaxis inducing potential of CCL19 and CCL19$^{CCL21\text{-}tail}$ compared to CCL21 is conferred by the CCL19 N-terminus (i.e., the receptor docking domain), we used another chimera in which the first 16 amino acids in CCL21 were exchanged with the equivalent part of CCL19; CCL21$^{CCL19\text{-}N\text{-}term}$. Since this chimera retains the low potency of CCL21 in chemotaxis assays, the N-terminus of CCL19 cannot alone be accountable for the higher potency of CCL19 and CCL19$^{CCL21\text{-}tail}$ compared to CCL21 in inducing directed migration.

In search for a common pathway relaying ligand potency to chemotaxis control, we tested signaling of all ligands in parallel for their ability to signal via ligand induced $G_{\alpha i}$ related changes in cAMP in CHO cells. Interestingly, transfer of CCL21-tail seems to negatively affect CCL19 signaling via cAMP with CCL19$^{CCL21\text{-}tail}$ displaying a 15-fold reduction in signaling through this pathway compared to CCL19, although CCL19$^{CCL21\text{-}tail}$ is still approximately 15-fold more potent than CCL21. Remarkably, removal of CCL21-tail in CCL21^{tailless}, results in improved signaling of CCL21 (~15-fold), making it equipotent to CCL19$^{CCL21\text{-}tail}$, indicating that tail alone to some degree inhibits signaling via cAMP. Like in chemotaxis, CCL21$^{CCL19\text{-}N\text{-}term}$ resembles CCL21 in cAMP signaling. The fact that CCL19 N-terminus does not rescue CCL21 cAMP signaling (in CCL21$^{CCL19\text{-}N\text{-}term}$), but if anything negatively affects CCL21 signaling again indicates that separate chemokine domains do not act independently and that CCL21-mediated CCR7 activation is probably not only determined by its N-terminus, but that tail interaction with CCR7 and possibly GAGs in the environment together with the core domain also affect CCL21-mediated CCR7 activation. Our data support that it is the CCL21-tail in combination with the CCL21 core domain that leaves CCL21 a less potent signaling molecule in these readouts compared to CCL19.

As summarized in Table 1, all chemokines tested in this study are potent in at least one readout (calcium, cAMP, CCR7 endocytosis, or 3D chemotaxis), except for CCL21$^{CCL19\text{-}N\text{-}term}$, and thus, in general, we believe that the effects we describe herein are not based on changes in CCR7 affinity between the chemokines tested, although this cannot be ruled out for CCL21$^{CCL19\text{-}N\text{-}term}$.

In a study by Kiermaier et al.[32] it was shown that CCL21 signaling is impaired due to an autoinhibitory function of the tail, that is envisioned to fold back on the chemokine, creating a locked autoinhibited CCL21 form, which is unlocked upon binding to polysialic acid residues on CCR7, that is, therefore, of importance for CCL21 induced CCR7 activity. This group found both CCL21 and CCL19$^{CCL21\text{-}tail}$ induced chemotaxis of murine DCs to be dependent on expression of polysialylation enzymes (including St8sia4) by the DCs.[32] NMR spectra suggest that there is a change in conformation between CCL21 and CCL21^{tailless} resulting from tail deletion suggesting that tail interactions with the core chemokine domain in CCL21 result in an autoinhibited state.[32] Whether this forced change in conformation is also occurring in CCL19$^{CCL21\text{-}tail}$ and therefore affects CCL19$^{CCL21\text{-}tail}$ activity was not addressed in this study.

In the current study, we do not address the effect of polysialylation on relief of tail induced autoinhibition as such but our data indicate that differences in overall chemokine structure relay variances in signaling strength that are polysialylation independent, as we show that CCL21 is less potent than CCL19$^{CCL21\text{-}tail}$ in inducing human DC migration, where polysialylation is expected to take place, and that it is also less potent than CCL19$^{CCL21\text{-}tail}$ in cAMP signaling in CHO cells that do not perform polysialylation.

In summary, we show that enhanced CCL21 tail-mediated binding of chemokines to the DC cell surface does not itself disturb ligand potency in chemotaxis and calcium signaling, although it negatively affects CCR7 internalization and CCR7 induced $G_{\alpha i}$ mediated reduction in cAMP. We also provide data supporting that it is the CCL21 core domain together with CCL21-tail that determines the low potency of CCL21 in CCR7 induced $G_{\alpha i}$ mediated reduction in cAMP. Chemotaxis is probably not governed via intracellular calcium signaling, whereas signaling via reduction of intracellular cAMP seems to be positively linked to migration as only the ligands that efficiently induce a decrease in cAMP seems to be able to induce migration with high potency (CCL19, CCL19$^{CCL21\text{-}tail}$, and CCL21^{tailless}).

Our observations support a role for CCL19 that displays enhanced endocytosis and thus CCR7 cell surface down-regulation compared to CCL21, in short-lived processes, for example, the DC-T cell scanning process in the LNs (with CCL19 being secreted by activated DCs) and CCL21 being important for the initial LN homing from peripheral tissues. The in vivo generated truncated form of CCL21, CCL21^{tailless} that is produced via the action of DC released proteases and is mainly potent in inducing chemotaxis, is suspected to potentiate DC LN homing when many DCs are activated at the same time, during serious infections.[42]

TABLE 1 Summarizes potencies of the ligands used in the study. +++ indicates high, ++ medium, + low and (+) very low potency. NA is abbreviation for Not Assayed.

Chemokine / Assay	CCL19	CCL21	$CCL19^{CCL21tail}$	$CCL21^{CCL19\text{-}Nterm}$	$CCL21^{tailless}$
$\uparrow[Ca^{2+}]_i$	++	+++	++	+	(+)
$\downarrow[cAMP]_i$	+++	+	++	(+)	++
CCR7 Endocytosis	+++	+	++	NA	NA
3D Chemotaxis	+++	+	+++	+	+++

In the current work, we focus on chemokine action in human DCs. There is reason to believe that chemokines may play different roles in different immune cell subtypes, thus $CCL21^{tailless}$ (soluble CCL21) has been shown to be moderately more potent but much less efficient in inducing chemotaxis of primary human T-cells compared to CCL21,[19] a fact that may be related to low heparan sulphate proteoglycan cell surface expression on unstimulated (quiescent) T-cells.[43,44] This is in contrast to human DCs, the chemotaxis of which is efficiently stimulated by $CCL21^{tailless}$, but less so by $CCL21^{14}$, and that are known to express high levels of heparin sulphate, both in immature and mature states.[45] Based on this, it will be interesting to investigate the action of the chemokines guiding DC LN homing and scanning processes for their action in human naïve T cells.

ACKNOWLEDGMENTS

This study was supported by research funding from the Gangsted Foundation, the AP Møller Foundation, and the Swiss National Science Foundation (grant No. 31003A_169936). J.M.L. is recipient of a stipend from the KoRS-CB. This material is based upon work supported by the National Science Foundation under grant No. 1400815. Any opinions, findings, and conclusions or recommendations expressed in this material are those of the author(s) and do not necessarily reflect the views of the National Science Foundation. We thank Allyson J. Fillmore for assistance in producing $CCL19^{CCL21\text{-}tail}$. We thank Francis C. Peterson for assistance with protein NMR data collection and the Medical College of Wisconsin NMR Facility for access to high field instruments.

AUTHORSHIP

G.M.H, A.S.J., C.T.V., and M.M.R designed the study. G.M.H., A.S.J., C.T.V., J.M.L., and D.F.L. performed research and/or analyzed data. P.E.A. and C.T.V. contributed vital reagents, $CCL19^{CCL21\text{-}tail}$ and $CCL21^{CCL19\text{-}N\text{-}term}$. G.M.H and M.M.R. interpreted data. G.M.H., A.S.J., and M.M.R. wrote the paper. All co-authors edited the manuscript.

DISCLOSURE

The authors declare no conflict of interest.

ORCID

Daniel F. Legler http://orcid.org/0000-0001-8610-4764
Mette M. Rosenkilde http://orcid.org/0000-0001-9600-3254
Gertrud M. Hjortø http://orcid.org/0000-0002-0057-6371

REFERENCES

1. Forster R, Davalos-Misslitz AC, Rot A. CCR7 and its ligands: balancing immunity and tolerance. *Nat Rev Immunol*. 2008;8:362–371.
2. Link A, Vogt TK, Favre S, et al. Fibroblastic reticular cells in lymph nodes regulate the homeostasis of naive T cells. *Nat Immunol*. 2007;8:1255–1265.
3. Worbs T, Mempel TR, Bolter J, von Andrian UH, Forster R. CCR7 ligands stimulate the intranodal motility of T lymphocytes in vivo. *J Exp Med*. 2007;204:489–495.
4. Kaiser A, Donnadieu E, Abastado JP, Trautmann A, Nardin A. CC chemokine ligand 19 secreted by mature dendritic cells increases naive T cell scanning behavior and their response to rare cognate antigen. *J Immunol*. 2005;175:2349–2356.
5. Wang Y, Irvine DJ. Convolution of chemoattractant secretion rate, source density, and receptor desensitization direct diverse migration patterns in leukocytes. *Integr Biol (Camb)*. 2013;5:481–494.
6. Sallusto F, Palermo B, Lenig D, et al. Distinct patterns and kinetics of chemokine production regulate dendritic cell function. *Eur J Immunol*. 1999;29:1617–1625.
7. Yoshida R, Nagira M, Kitaura M, Imagawa N, Imai T, Yoshie O. Secondary lymphoid-tissue chemokine is a functional ligand for the CC chemokine receptor CCR7. *J Biol Chem*. 1998;273:7118–7122.
8. Yoshida R, Imai T, Hieshima K, et al. Molecular cloning of a novel human CC chemokine EBI1-ligand chemokine that is a specific functional ligand for EBI1, CCR7. *J Biol Chem*. 1997;272:13803–13809.
9. Hauser MA, Legler DF. Common and biased signaling pathways of the chemokine receptor CCR7 elicited by its ligands CCL19 and CCL21 in leukocytes. *J Leukoc Biol*. 2016;99:869–882.
10. Luther SA, Tang HL, Hyman PL, Farr AG, Cyster JG. Coexpression of the chemokines ELC and SLC by T zone stromal cells and deletion of the ELC gene in the plt/plt mouse. *Proc Natl Acad Sci USA*. 2000;97:12694–12699.
11. Carlsen HS, Haraldsen G, Brandtzaeg P, Baekkevold ES. Disparate lymphoid chemokine expression in mice and men: no evidence of CCL21 synthesis by human high endothelial venules. *Blood*. 2005;106:444–446.
12. Ngo VN, Tang HL, Cyster JG. Epstein-Barr virus-induced molecule 1 ligand chemokine is expressed by dendritic cells in lymphoid tissues and strongly attracts naive T cells and activated B cells. *J Exp Med*. 1998;188:181–191.
13. Katou F, Ohtani H, Nakayama T, Nagura H, Yoshie O, Motegi K. Differential expression of CCL19 by DC-Lamp+ mature dendritic cells in human lymph node versus chronically inflamed skin. *J Pathol*. 2003;199:98–106.
14. Hjorto GM, Larsen O, Steen A, et al. Differential CCR7 Targeting in dendritic cells by three naturally occurring CC-Chemokines. *Front Immunol*. 2016;7:568.
15. Zidar DA, Violin JD, Whalen EJ, Lefkowitz RJ. Selective engagement of G protein coupled receptor kinases (GRKs) encodes distinct functions of biased ligands. *Proc Natl Acad Sci USA*. 2009;106:9649–9654.

16. Kohout TA, Nicholas SL, Perry SJ, Reinhart G, Junger S, Struthers RS. Differential desensitization, receptor phosphorylation, beta-arrestin recruitment, and ERK1/2 activation by the two endogenous ligands for the CC chemokine receptor 7. *J Biol Chem*. 2004;279:23214–23222.
17. Otero C, Groettrup M, Legler DF. Opposite fate of endocytosed CCR7 and its ligands: recycling versus degradation. *J Immunol*. 2006;177:2314–2323.
18. Byers MA, Calloway PA, Shannon L, et al. Arrestin 3 mediates endocytosis of CCR7 following ligation of CCL19 but not CCL21. *J Immunol*. 2008;181:4723–4732.
19. Hauser MA, Kindinger I, Laufer JM, et al. Distinct CCR7 glycosylation pattern shapes receptor signaling and endocytosis to modulate chemotactic responses. *J Leukoc Biol*. 2016;99:993–1007.
20. Ricart BG, John B, Lee D, Hunter CA, Hammer DA. Dendritic cells distinguish individual chemokine signals through CCR7 and CXCR4. *J Immunol*. 2011;186:53–61.
21. Steen A, Thiele S, Guo D, Hansen LS, Frimurer TM, Rosenkilde MM. Biased and constitutive signaling in the CC-chemokine receptor CCR5 by manipulating the interface between transmembrane helices 6 and 7. *J Biol Chem*. 2013;288:12511–12521.
22. Steen A, Sparre-Ulrich AH, Thiele S, Guo D, Frimurer TM, Rosenkilde MM. Gating function of isoleucine-116 in TM-3 (position III:16/3.40) for the activity state of the CC-chemokine receptor 5 (CCR5). *Br J Pharmacol*. 2014;171:1566–1579.
23. Steen A, Larsen O, Thiele S, Rosenkilde MM. Biased and g protein-independent signaling of chemokine receptors. *Front Immunol*. 2014;5:277.
24. Love M, Sandberg JL, Ziarek JJ, etal. Solution structure of CCL21 and identification of a putative CCR7 binding site. *Biochemistry*. 2012;51:733–735.
25. Schwartz TW, Frimurer TM, Holst B, Rosenkilde MM, Elling CE. Molecular mechanism of 7TM receptor activation–a global toggle switch model. *Annu Rev Pharmacol Toxicol*. 2006;46:481–519.
26. Rosenkilde MM, Benned-Jensen T, Frimurer TM, Schwartz TW. The minor binding pocket: a major player in 7TM receptor activation. *Trends Pharmacol Sci*. 2010;31:567–574.
27. Ott TR, Pahuja A, Nickolls SA, Alleva DG, Struthers RS. Identification of CC chemokine receptor 7 residues important for receptor activation. *J Biol Chem*. 2004;279:42383–42392.
28. Gaieb Z, Morikis D. Conformational heterogeneity in CCR7 undergoes transitions to specific states upon ligand binding. *J Mol Graph Model*. 2017;74:352–358.
29. Patel DD, Koopmann W, Imai T, Whichard LP, Yoshie O, Krangel MS. Chemokines have diverse abilities to form solid phase gradients. *Clin Immunol*. 2001;99:43–52.
30. Hirose J, Kawashima H, Yoshie O, Tashiro K, Miyasaka M. Versican interacts with chemokines and modulates cellular responses. *J Biol Chem*. 2001;276:5228–5234.
31. Barmore AJ, Castex SM, Gouletas BA, et al. Transferring the C-terminus of the chemokine CCL21 to CCL19 confers enhanced heparin binding. *Biochem Biophys Res Commun*. 2016;477:602–606.
32. Kiermaier E, Moussion C, Veldkamp CT, et al. Polysialylation controls dendritic cell trafficking by regulating chemokine recognition. *Science*. 2016;351:186–190.
33. Lorenz N, Loef EJ, Kelch ID, et al. Plasmin and regulators of plasmin activity control the migratory capacity and adhesion of human T cells and dendritic cells by regulating cleavage of the chemokine CCL21. *Immunol Cell Biol*. 2016;94:955–963.
34. Schumann K, Lammermann T, Bruckner M, et al. Immobilized chemokine fields and soluble chemokine gradients cooperatively shape migration patterns of dendritic cells. *Immunity*. 2010;32:703–713.
35. Veldkamp CT, Koplinski CA, Jensen DR, et al. Production of recombinant chemokines and validation of refolding. *Methods Enzymol*. 2016;570:539–565.
36. Veldkamp CT, Kiermaier E, Gabel-Eissens SJ, et al. Solution structure of CCL19 and identification of overlapping CCR7 and PSGL-1 binding sites. 2015;54:4163–4166.
37. Otero C, Eisele PS, Schaeuble K, Groettrup M, Legler DF. Distinct motifs in the chemokine receptor CCR7 regulate signal transduction, receptor trafficking and chemotaxis. *J Cell Sci*. 2008;121:2759–2767.
38. Jiang LI, Collins J, Davis R, et al. Use of a cAMP BRET sensor to characterize a novel regulation of cAMP by the sphingosine 1-phosphate/G13 pathway. *J Biol Chem*. 2007;282:10576–10584.
39. Amarandi RM, Hjorto GM, Rosenkilde MM, Karlshoj S. Probing biased signaling in chemokine receptors. *Methods Enzymol*. 2016;570:155–186.
40. Hirose J, Kawashima H, Swope WM, et al. Chondroitin sulfate B exerts its inhibitory effect on secondary lymphoid tissue chemokine (SLC) by binding to the C-terminus of SLC. *Biochim Biophys Acta*. 2002;1571:219–224.
41. Gaieb Z, Lo DD, Morikis D. molecular mechanism of biased ligand conformational changes in CC chemokine receptor 7. *J Chem Inf Model*. 2016;56:1808–1822.
42. Jorgensen AS, Rosenkilde MM, Hjorto GM. Biased signaling of G protein-coupled receptors - From a chemokine receptor CCR7 perspective. *Gen Comp Endocrinol*. 2018;258:4–14.
43. Jones KS, Petrow-Sadowski C, Bertolette DC, Huang Y, Ruscetti FW. Heparan sulfate proteoglycans mediate attachment and entry of human T-cell leukemia virus type 1 virions into CD4+ T cells. *J Virol*. 2005;79:12692–12702.
44. Rueda P, Balabanian K, Lagane B, et al. The CXCL12gamma chemokine displays unprecedented structural and functional properties that make it a paradigm of chemoattractant proteins. *PLoS One*. 2008;3:e2543.
45. Wegrowski Y, Milard AL, Kotlarz G, Toulmonde E, Maquart FX, Bernard J. Cell surface proteoglycan expression during maturation of human monocytes-derived dendritic cells and macrophages. *Clin Exp Immunol*. 2006;144:485–493.

SUPPORTING INFORMATION

Additional information may be found online in the supporting information tab for this article.

How to cite this article: Jørgensen AS, Adogamhe PE, Laufer JM, et al. CCL19 with CCL21-tail displays enhanced glycosaminoglycan binding with retained chemotactic potency in dendritic cells. *J Leukoc Biol*. 2018;104:401–411. https://doi.org/10.1002/JLB.2VMA0118-008R